Simulation of nonlinear Compton scattering from bound electrons

Akilesh Venkatesh and Francis Robicheaux ⬤

Department of Physics and Astronomy, Purdue University, West Lafayette, Indiana 47907, USA

Recent investigations by Fuchs *et al.* [Matthias Fuchs, Mariano Trigo, Jian Chen, Shambhu Ghimire, Sharon Shwartz, Michael Kozina, Mason Jiang, Thomas Henighan, Crystal Bray, Georges Ndabashimiye *et al.*, Anomalous nonlinear X-ray Compton scattering, Nat. Phys. **11**, 964 (2015)] revealed an anomalous frequency shift in nonlinear Compton scattering of high-intensity x rays by electrons in solid beryllium. This frequency shift was at least 800 eV to the red of the values predicted by analytical free-electron models for the same process. In this paper, we describe a method for simulating nonlinear Compton scattering. The method is applied to the case of bound electrons in a local, spherical potential to explore the role of binding energy in the frequency shift of scattered x rays for different scattered angles. The results of the calculation do not exhibit an additional redshift for the scattered x rays beyond the nonlinear Compton shift predicted by the free-electron model. However, they do reveal a small blueshift relative to the free-electron prediction for nonlinear Compton scattering. The effect of electron-electron correlation effects is calculated and determined to be unlikely to be the source of the redshift. The case of linear Compton scattering from a photoionized electron followed by electron recapture is examined as a possible source of the redshift and ruled out.

I. INTRODUCTION

Since, the discovery of Compton scattering 90 years ago, various measurements have been carried out to confirm the results to a higher accuracy and to probe the finer details of the Compton spectrum [1,2]. This has given rise to the study of Compton profiles which provide extensive information about the momentum distribution of the electrons involved in the scattering [3,4]. Compton profiles have also proven useful as an experimental check on the accuracy of the ground-state wave function of electrons in momentum space obtained through theoretical methods. A number of applications in areas from material science to astrophysics have been born out of these studies [5,6].

In this paper, nonlinear Compton scattering refers to the process where two incoming photons interact with an electron, leading to one outgoing photon. Nonlinear Compton scattering was first described by Brown and Kibble [7] in 1964, where they developed an analytical QED framework to model the nonlinear scattering [8] of photons by a free electron. In their work, they showed that when nonlinear Compton scattering occurs, for the nonrelativistic case, the frequency of the scattered photon can be obtained by the usual Compton expression, provided one replaces the incoming frequency by twice that value. Including relativistic effects in the calculation gives rise to ponderomotive forces on the electron. At extremely high intensities (electric field > 10 000 a.u. for x rays), the ponderomotive effects lead to the electron behaving as if it had a smaller mass and thus producing a bigger redshift for the scattered photons. It was more than two decades before experiments could study nonlinear x-ray–matter interactions, but the arrival of x-ray free-electron lasers [9,10] has made considerable progress [11,12] possible.

More recently, Fuchs *et al.* [13] carried out an experiment to investigate nonlinear x-ray–matter interactions with the Linac Coherent Light Source at the SLAC National Accelerator Laboratory. They used a high-intensity x-ray free-electron laser to study nonlinear scattering from solid beryllium. While nonlinear Compton scattering had been earlier observed [14], Fuchs *et al.* [13] found a nonlinear Compton signal that was substantially redshifted from the value predicted by Brown and Kibble [7]. To explain this additional redshift (≈ 800 eV), they proposed that the bound nature of the beryllium electrons could be responsible. This argument was analyzed by Krebs *et al.* [15]. They solved the time-dependent Schrödinger equation (TDSE) to simulate the nonlinear x-ray scattering, with the bound electrons being modeled by a potential based on the Hartree-Fock-Slater model. Their calculations did not reveal any anomalies with respect to the free-electron results.

In this paper, we reexamine the additional frequency shift in Fuchs *et al.* [13]. We use a numerical approach different from that of Ref. [15] and study the effect of binding energy (BE), electron-electron correlation, and photoionization on the nonlinear Compton spectrum. We were able to obtain convergent results for both the differential cross section and the average scattered photon momentum for both linear Compton and nonlinear Compton scattering. While we mainly agree with the results of Krebs *et al.* [15], our calculations reveal a small blueshift in the frequency of the scattered photon with respect to the free-electron results. Following this, we explore two possible alternate causes for the redshift. First, we consider the role of electron-electron correlation effects on the scattering profile. Second, we examine the possibility of a semi-Compton process to give rise to the anomalous redshift.

For free electrons, we performed calculations where the electron part of the wave function was restricted to two dimensions, but for most of the bound-electron calculations the electron was fully three-dimensional (3D). For a given number of dimensions, the calculation for a bound electron involves

less time and space computationally than its free-electron counterpart. It should be noted that a two-dimensional (2D) model is quite adequate to describe both linear and nonlinear Compton scattering but the exact factors required to calculate the differential cross length is not well defined. The 3D simulations lead to results with no adjustable parameters.

The model's validity is demonstrated by reproducing the differential cross length of x-ray scattering from a free electron from a QED-2+1 scheme, which is a 2D analog of the Klein-Nishina formula [16,17]. Another way the validity of the model is tested is by comparing it with the nonlinear Compton differential cross section of Brown and Kibble [7] for small binding energy. Finally the model is applied to the x-ray-scattering scenario in Fuchs *et al.* [13] to study both Compton and nonlinear Compton scattering from a bound electron. In our calculations, we consider a range of binding energies for the bound electrons from 0.4 to 6 a.u. This range of binding energies is relevant for Be because the atomic Be has an ionization potential of 0.34 a.u. and that of Be^{2+} is 5.6 a.u.

Unless otherwise stated, atomic units will be used throughout this paper.

II. METHODS AND MODELING

The first step in our approach is to model the initial state of the electron. For the free-electron case, we use a Gaussian wave packet as the initial state. Recently, Pan and Gover [18] while analyzing spontaneous and stimulated emissions found that the size of the initial wave packet has nontrivial effects on the spectrum of the outgoing photons. These effects appear when the outgoing photons are in a coherent state and not a Fock state. However, for the scattering problem under consideration, the size of the Gaussian wave packet is not significant.

For the bound-electron case, we treat the electron as an atomic single electron and model the rest of the atom with an effective time-independent, local potential. We solve the time-independent Schrödinger equation to obtain the ground-state spatial wave function. For this, we use the relaxation method, propagating the Schrödinger equation in imaginary time until only the ground state remains. The ground-state wave function, thus obtained, was the initial state of the bound electrons in our calculations.

With the appropriate initial wave function, we can compute the time-dependent wave function for the electron in a classical field by numerically solving the TDSE. To model the scattered photon, we employ lowest-order perturbation theory and solve for the case of a single outgoing photon. We obtain the scattering probability for different angles, which is used to calculate the differential cross section as a function of angle.

The nonrelativistic treatment of the electron implied by the TDSE should be accurate enough for the conditions below. Consider the case of nonlinear Compton scattering of a photon of $w = 340$ a.u. from a free electron. Even for the case of back scattering, the electron would at most gain approximately 1.2 keV of energy from the photon [Eq. (22)]. From the experiment by Fuchs *et al.* [13], we expect an additional kinetic-energy gain of approximately 1 keV. Together, that would still give a Lorentz factor(γ) of only 1.004 which is well within

the nonrelativistic regime. As a check on the approximation, we consider the lowest-order relativistic correction to the Schrödinger equation in Sec. II B and demonstrate that it hardly changes the overall results.

A. Deriving the nonhomogeneous Schrödinger equation

We model the vector potential by treating the incoming electromagnetic (EM) wave classically and quantizing the scattered wave [19]:

$$\hat{A} = A_C + \hat{A}_Q. \tag{1}$$

Here, $\hat{A}$ is the total vector potential. The quantities A_C and $\hat{A}_Q$ refer to the classical vector potential and the quantized vector potential, respectively. The quantized vector potential is given by [19]

$$\hat{A}_Q = \sqrt{\frac{2\pi}{V}} \sum_{k,\epsilon} \frac{1}{\sqrt{\omega_k}} [\epsilon e^{ik \cdot r} \hat{a}_{k,\epsilon} + \epsilon^* e^{-ik \cdot r} \hat{a}^\dagger_{k,\epsilon}]. \tag{2}$$

The symbols ϵ and k refer to the unit polarization vector and wave vector of the photon, respectively, with $k \cdot \epsilon = 0$. Here, $\omega_k = |k|c$. The operators $\hat{a}^\dagger_{k,\epsilon}$ and $\hat{a}_{k,\epsilon}$ can create or annihilate a photon in mode (k, ϵ), respectively. The V in the prefactor refers to the volume of the region used to quantize the electromagnetic field modes. The quantity r is the position vector and c is the speed of light in vacuum, which is approximately 137.036 a.u. It is to be noted that the final results are independent of the quantization volume V, because we consider the limit of an infinite volume.

The classical vector potential is modeled as a laser pulse with linear polarization. We choose the coordinate system such that the electric field only has a y component and the x-ray pulse propagates in the x direction. Our choice for this is given by the vector potential:

$$A_C = \frac{E_C}{\omega_{in}} \cos\left[\omega_{in}\left(t - \frac{x}{c}\right)\right] \exp\left[\frac{\left[-2\ln 2\left(t - \frac{x}{c}\right)^2\right]}{t^2_{wid}}\right] \hat{y}. \tag{3}$$

Here E_C and ω_{in} refer to the amplitude and the angular frequency of the incoming electric field, respectively, and t_{wid} indicates the full width at half maximum of the pulse intensity. It is to be noted that A_C is a function of x and t only.

For the light-matter interaction, the Hamiltonian [20] is

$$\hat{H} = \frac{(\hat{P} + \hat{A})^2}{2} + V(\hat{x}) + \sum_{k,\epsilon} \omega_k \hat{a}^\dagger_{k,\epsilon} \hat{a}_{k,\epsilon}. \tag{4}$$

Note that the exact form of the potential energy $V(\hat{x})$ is discussed in Sec. III. We use Eqs. (1), (2), and (4) and separate out the terms with and without $\hat{A}_Q$. The terms with $\hat{A}_Q$ are part of the perturbative correction. In this paper, we retain only the terms of first order in $\hat{A}_Q$. One reason for this is that the higher-order terms give rise to two scattered photons and the Lamb shift, both of which are beyond the scope of this paper. Thus, our unperturbed Hamiltonian is

$$\hat{H}^{(0)} = \frac{(\hat{P} + A_C)^2}{2} + V(\hat{x}) + \sum_{k,\epsilon} \omega_k \hat{a}^\dagger_{k,\epsilon} \hat{a}_{k,\epsilon}. \tag{5}$$

The perturbation term is

$$\hat{H}^{(1)} = (\hat{\boldsymbol{P}} + \boldsymbol{A}_C) \cdot \hat{\boldsymbol{A}}_Q. \tag{6}$$

The wave function is expanded in the Fock basis based on the number of scattered photons. Therefore our wave-function ansatz is as follows:

$$|\psi_{\text{total}}\rangle = \psi^{(0)}(\boldsymbol{r}, t) |0\rangle + \sum_{\boldsymbol{k}, \boldsymbol{\epsilon}} \psi^{(1)}_{\boldsymbol{k}, \boldsymbol{\epsilon}}(\boldsymbol{r}, t) e^{-i\omega_k t} \hat{a}^{\dagger}_{\boldsymbol{k}, \boldsymbol{\epsilon}} |0\rangle \tag{7}$$

where $|0\rangle$ refers to the vacuum state of the photon in Fock space. The ansatz is adequate because the first term describes an electron interacting with a classical EM field without any scattered photons. The wave function of this electron is given by $\psi^{(0)}(\boldsymbol{r}, t)$. The second term describes the presence of a scattered photon. The quantity $\psi^{(1)}_{\boldsymbol{k}, \boldsymbol{\epsilon}}(\boldsymbol{r}, t)$ is the probability amplitude at time t, for a photon to scatter into momentum $\boldsymbol{k}$ and polarization $\boldsymbol{\epsilon}$ and the electron to be found at position $\boldsymbol{r}$.

Given the Hamiltonian and the wave-function ansatz, we proceed with the TDSE retaining only the terms up to first order in perturbation and separating out the equations based on the number of scattered photons. For no scattered photons,

$$i\frac{\partial \psi^{(0)}}{\partial t} - \hat{H}_C \psi^{(0)} = 0 \tag{8}$$

where

$$\hat{H}_C = \hat{H}^{(0)} - \sum_{\boldsymbol{k}, \boldsymbol{\epsilon}} \omega_k \hat{a}^{\dagger}_{\boldsymbol{k}, \boldsymbol{\epsilon}} \hat{a}_{\boldsymbol{k}, \boldsymbol{\epsilon}}. \tag{9}$$

Note that $\hat{H}_C$ appears in Eq. (8) because $\psi^{(0)}$ is defined as the wave function of an electron interacting with a classical EM field. For one scattered photon we get

$$i\frac{\partial \psi^{(1)}_{\boldsymbol{k}, \boldsymbol{\epsilon}}}{\partial t} - \hat{H}_C \psi^{(1)}_{\boldsymbol{k}, \boldsymbol{\epsilon}} = \sqrt{\frac{2\pi}{V\omega_k}} e^{-i\boldsymbol{k}\cdot\boldsymbol{r}} e^{i\omega_k t}$$
$$\times \, \boldsymbol{\epsilon}^* \cdot (\hat{\boldsymbol{P}} + \boldsymbol{A}_C) W(t) \psi^{(0)} \tag{10}$$

where

$$W(t) = e^{-\left(\frac{t}{\tau}\right)^8}. \tag{11}$$

The windowing function, $W(t)$, adiabatically turns on the inhomogeneous term in Eq. (10) only for the duration of the incident laser pulse, t_{wid}. This is done to find the ground state of the electron-photon coupled system. This also prevents the unphysical emission of photons, that would occur if the interaction between the electron and quantized photons was instantaneously turned on. Note that the function should be smooth to avoid encountering the Gibbs phenomenon [21]. The choice of τ is determined by the duration of the pulse. The results of the calculation do not depend on τ as long as $\tau > 3.2\, t_{\text{wid}}$ approximately. Another competing consideration is that τ should be as small as possible to ensure that we only need to solve the TDSE for a short duration. In our calculations we chose $\tau \sim 3.2\, t_{\text{wid}}$. The results do not depend on the specific choice of the windowing function as long as it is a smooth function which attains a value of 1, only during the duration of the incoming pulse.

A modification of the procedure developed in this subsection is considered in Sec. III C where the results of a two-electron calculation are discussed to probe electron-electron correlation effects in two dimensions.

B. Relativistic correction: $(P + A)^4$ terms

Here, we demonstrate how a relativistic correction may be implemented. We do this by considering the next-higher-order term in mechanical momentum and rederiving the expressions in Eqs. (8) and (10). A careful consideration of the non-commuting terms in $(\hat{\boldsymbol{P}} + \hat{\boldsymbol{A}})^4$ is required to derive the new equations. For no scattered photons,

$$i\frac{\partial \psi^{(0)}}{\partial t} - \hat{H}_C \psi^{(0)} = -\frac{1}{8c^2}(\hat{\boldsymbol{P}} + \boldsymbol{A}_C)^4 \psi^{(0)}. \tag{12}$$

For one scattered photon,

$$i\frac{\partial \psi^{(1)}_{\boldsymbol{k}, \boldsymbol{\epsilon}}}{\partial t} - \hat{H}_C \psi^{(1)}_{\boldsymbol{k}, \boldsymbol{\epsilon}} = -\frac{1}{8c^2}(\hat{\boldsymbol{P}} + \boldsymbol{A}_C)^4 \psi^{(1)}_{\boldsymbol{k}, \boldsymbol{\epsilon}}$$
$$+ \sqrt{\frac{2\pi}{V\omega_k}} \boldsymbol{\epsilon}^* \cdot \left[e^{-i\boldsymbol{k}\cdot\boldsymbol{r}} e^{i\omega_k t}(\hat{\boldsymbol{P}} + \boldsymbol{A}_C) - \frac{1}{2c^2} e^{i\omega_k t} \hat{\boldsymbol{G}} \right] \psi^{(0)} \tag{13}$$

where

$$\hat{\boldsymbol{G}} = [e^{-i\boldsymbol{k}\cdot\boldsymbol{r}}(\hat{\boldsymbol{P}} + \boldsymbol{A}_C)^3] + [(\hat{\boldsymbol{P}} + \boldsymbol{A}_C)^3 e^{-i\boldsymbol{k}\cdot\boldsymbol{r}}]$$
$$+ [(\hat{\boldsymbol{P}} + \boldsymbol{A}_C)^2 e^{-i\boldsymbol{k}\cdot\boldsymbol{r}}(\hat{\boldsymbol{P}} + \boldsymbol{A}_C)]$$
$$+ [(\hat{\boldsymbol{P}} + \boldsymbol{A}_C) e^{-i\boldsymbol{k}\cdot\boldsymbol{r}}(\hat{\boldsymbol{P}} + \boldsymbol{A}_C)^2]. \tag{14}$$

The above equations are a simple way in which relativistic corrections can be implemented. An alternative, more sophisticated approach would be to use the relativistic Schrödinger equation [22]. However, there is no need for such an approach given the results in Sec. III A. If the fields were a few orders of magnitude higher, there would be a need for a more sophisticated treatment of relativistic corrections [23].

C. Differential cross section

The probability for a photon to scatter with momentum $\boldsymbol{k}$ and polarization $\boldsymbol{\epsilon}$ is

$$P_{\boldsymbol{k}, \boldsymbol{\epsilon}} = \int_v \psi^{(1)*}_{\boldsymbol{k}, \boldsymbol{\epsilon}} \psi^{(1)}_{\boldsymbol{k}, \boldsymbol{\epsilon}} d^n r. \tag{15}$$

Here $d^n r$ refers to the volume element in n dimensions.

The method described in Sec. II A automatically leads to a spread in the scattered photon momentum because the incoming field is not strictly monochromatic but rather a pulse. The amount of the spread in scattered photon momentum is determined by the width of the chosen laser pulse. Since there is a momentum spread in the scattered x ray, the differential cross section for a given scattering angle is a summation over all possible magnitudes of scattered photon momentum. The total one-photon cross section in three dimensions is given by

$$\sigma^{(1)} = \sum_{\boldsymbol{k}, \boldsymbol{\epsilon}} \frac{P_{\boldsymbol{k}, \boldsymbol{\epsilon}}}{(\text{number of photons/area})} \tag{16}$$

where [19]

$$\sum_{\boldsymbol{k}} \longrightarrow \frac{V}{(2\pi)^3} \int d^3 k \tag{17}$$

and

$$\frac{\text{number of photons}}{\text{area}} = \frac{\int I dt}{\omega_{\text{in}}}. \tag{18}$$

Here I refers to the intensity of the incoming field. It is to be noted that the incoming pulse is assumed to be quasi-monochromatic. This leads to the definition of the differential cross section:

$$\frac{d\sigma^{(1)}}{d\Omega} = \frac{V\omega_{\text{in}}}{(2\pi)^3} \frac{\int \sum_\epsilon P_{k,\epsilon} k^2 dk}{\int I dt}. \tag{19}$$

Here V is the quantization volume. There exists a factor of $1/V$ in $P_{k,\epsilon}$ which cancels out the V in the numerator. Note that ω_{in} refers to the angular frequency of the incoming electric field [Eq. (3)].

The two-photon cross section in three dimensions has been defined in multiple ways [24,25]. Here we define it so that the SI units would be $m^2/(W/m^2)$:

$$\sigma^{(2)} = \omega_{\text{in}} \frac{\sum_{k,\epsilon} P_{k,\epsilon}}{\int I^2 dt}. \tag{20}$$

Therefore the differential cross section would be

$$\frac{d\sigma^{(2)}}{d\Omega} = \frac{V\omega_{\text{in}}}{(2\pi)^3} \frac{\int \sum_\epsilon P_{k,\epsilon} k^2 dk}{\int I^2 dt}. \tag{21}$$

In both the one-photon and two-photon differential cross sections, we calculate these integrals with respect to $k^2 dk$ by doing a Gaussian fit for the plots of $P_{k,\epsilon}$ vs k and then performing an integral of the Gaussian function. The differential cross sections obtained from the 3D calculations do not have any adjustable parameters.

The exact factors to obtain the differential cross length from the scattering probability in two dimensions are not well defined. Therefore, we obtain this factor by scaling our differential cross sections to get an overall fit with the analytical free-electron results [7,16].

D. Solving the TDSE

We solve the TDSE using a Cartesian coordinate system with the wave function represented on a grid of points. The values of the grid parameters are specified in Sec. II E. For the kinetic-energy operator in the Hamiltonian, we use a three-point central difference formula. The TDSE for $\psi^{(0)}(\mathbf{r}, t)$ [Eq. (8)] is solved using the leap-frog method [26]. We choose the leap-frog method for two reasons: first, it preserves unitarity; second, it leads to converged results, which is discussed in detail in Sec. II E. The leap-frog method involves computing the wave function, which is two time steps ahead of the current wave function, using the wave function at the current time step and the wave function at the intermediate time. The second-order Runge-Kutta method is used to obtain the value of the wave function at the first time step which is required for the leap-frog approach. At every time instance, we simultaneously solve for $\psi^{(1)}_{k,\epsilon}(\mathbf{r}, t)$ for a range of scattered photon momenta centered around the Compton momentum or the Brown and Kibble prediction [Eq. (22)] for the linear Compton or nonlinear Compton, respectively. The plot of $P_{k,\epsilon}$ [Eq. (15)] as a function of scattered photon momentum k is a Gaussian curve (see Fig. 1) to a good approximation.
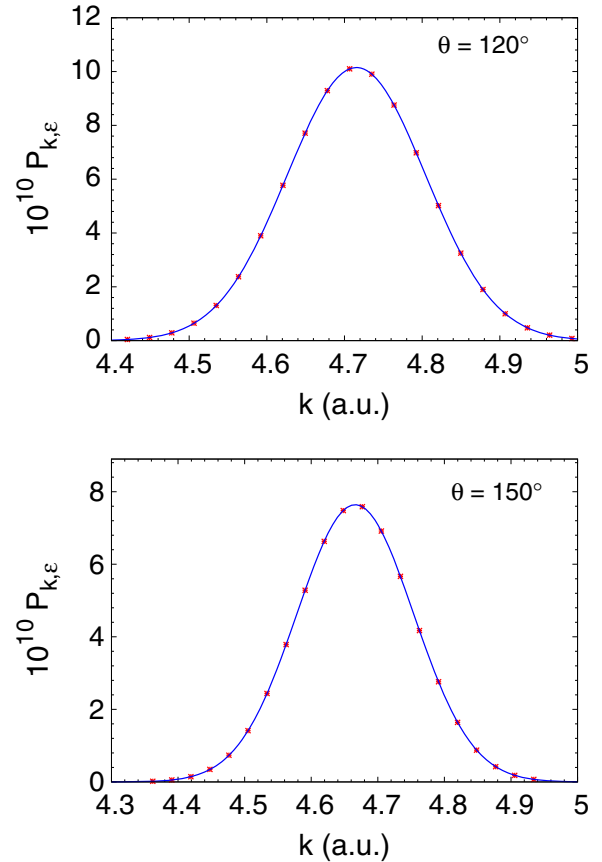

FIG. 1. Scattering probability $P_{k,\epsilon}$ as a function of scattered photon momentum k for nonlinear Compton calculations in two dimensions for an angle of $120°$ and $150°$, respectively, for a free electron. The red points indicate the results of the numerical calculation and the blue line indicates a Gaussian fit. The calculations were performed over an equal number of k values on either side of the theoretical value. Note that the peaks are at the expected nonlinear Compton momentum [Eq. (22)]. This calculations were done with $E_C = 107$ a.u., $\omega_{\text{in}} = 340$ a.u., and $t_{\text{wid}} = 0.125$ a.u.

In all our calculations unless otherwise stated, we use electric field $E_C = 107$ a.u. and angular frequency $\omega_{\text{in}} = 340$ a.u. for the incident laser pulse. In SI units, these values correspond to an electric field of $\approx 5 \times 10^{13}$ V/m and an intensity of $\approx 3 \times 10^{24}$ W/m². The chosen angular frequency corresponds to an incoming photon energy of about 9.25 keV. These values belong to the range used in the experiment by Fuchs *et al.* [13].

E. Grid and other numerical parameters

In our calculations, convergence is measured in two ways, by calculating the area under $P_{k,\epsilon}$ vs k plots and by calculating the change in the peak position of the scattering probability. For all the calculations except in Sec. III C, the change in this area with respect to change in grid spacing or grid size was under 2%. The change in the peak position of scattering probability with respect to change in grid spacing or grid size was under 0.5%.

For the 2D free-electron calculations, a grid size of 400×400 with a grid spacing of 0.1 a.u. in both x and y directions

resulted in converged results. For the 3D calculations with $Z = 1$ and 2 a grid range of $400 \times 400 \times 400$ with a grid spacing of 0.1 a.u. resulted in converged results. For $Z = 4$ a grid range of $229 \times 229 \times 229$ with a grid spacing of 0.07 units resulted in converged results.

The primary source of error in scattered photon momentum arises from the kinetic-energy operator. The leading-order error term is proportional to the square of the grid spacing. For the case of nonlinear Compton scattering from a bound electron at an angle of $130°$ and for a grid spacing of 0.07 a.u., the error is of the size of about 3% of the nonlinear Compton shift. This error is much smaller than the size of the anomalous shift observed in Ref. [13], which is about 100% of the Compton shift. In Sec. III B, we take our estimate for scattered photon momentum, k, below this 3% error by using Richardson's extrapolation to eliminate the leading-order error term.

For t_{wid}, we use a range of 0.1–1 a.u. which corresponds to a pulse of duration $\approx 10^{-18}$ s. The use of such a short pulse is justified because the results for the differential cross section are found to be independent of the choice of t_{wid}. A small change in peak scattered momentum is observed for different pulse widths. The magnitude of this change is less than about 1% of the momentum shift observed by Fuchs *et al.* [13]. Also, for the chosen range of t_{wid}, there is no reflection of the wave function from the walls, as the distance traveled by the wave packet of the electron is much smaller than the size of the grid.

III. APPLICATION

A. Free-electron case

We apply the method developed in Sec. II, to a free electron interacting with a laser pulse in two dimensions and compare the results of our calculation with the equivalent of the Klein-Nishina formula in two dimensions [16]. Note that the Klein-Nishina formula and its analog in two dimensions are derived for monochromatic radiation. Since we employ a pulse, we evaluate the integral $D = \int \sum_{\epsilon} P_{k,\epsilon} k \, dk$ to find a quantity proportional to the differential cross length for a given intensity and incoming frequency. We compute this quantity D for different angles and compare this with the differential cross length from the QED-2+1 scheme [16] and the differential cross section from Brown and Kibble [7]. From this point in our discussions, we will refer to D as the differential cross length for convenience keeping in mind that the calculation has been scaled to match the analytical result.

We plot the differential cross length we obtained for linear Compton as a function of angle and the results from QED-2+1 [16] in Fig. 2. Upon comparison, we find that our calculated differential cross length agrees well with the free-electron analytical results.

Next, we compare the calculated 2D differential cross length (see Fig. 3) for nonlinear Compton scattering with the analytical expression from Brown and Kibble [7]. We also evaluate the differential cross lengths using the relativistic corrections developed in Sec. II B for comparison. The procedure for scaling the differential cross length used previously is employed here as well. According to Brown and Kibble [7], for nonlinear Compton scattering, the frequency of the scattered photon using a nonrelativistic approximation
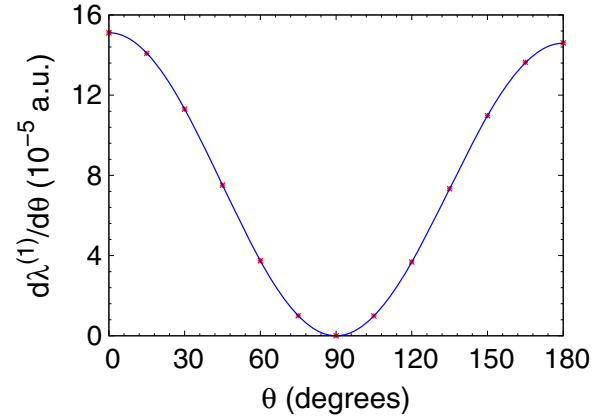

FIG. 2. Comparison of differential cross lengths as a function of angle subtended by the detector with the analog of the Klein-Nishina formula for two dimensions [16] for linear Compton scattering. The red points are the results of the numerical calculation and the blue line represents the results from the analytical expression [16]. The results of the numerical calculations in two dimensions were scaled by a single factor. This factor was chosen such that, overall, the numerical results fit well with the analytical results. The above calculations were done with the same parameters as Fig. 1.

is given by

$$\omega = \frac{n\omega_{in}}{1 + n\alpha^2 \omega_{in}(1 - \cos\theta)}. \quad (22)$$

Here, n determines the order of the process, for example, $n = 1$ for Compton scattering. The discussions in this paper are restricted to processes where $n \leqslant 2$. The symbols ω and ω_{in} refer to the angular frequency of the scattered photon and incoming photon, respectively, and α is the fine-structure constant.
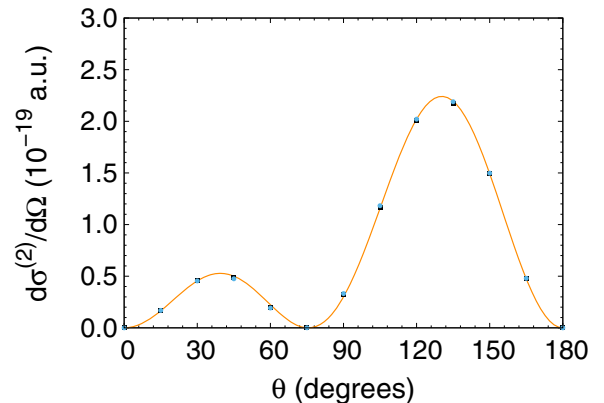

FIG. 3. Comparison of differential cross sections (lengths) as a function of scattering angle in two dimensions with the results of Brown and Kibble for nonlinear Compton scattering. The blue points indicate the nonrelativistic results obtained using Eqs. (8) and (10). The black squares were obtained using the approach from Sec. II B. The orange line indicates the result from Brown and Kibble. The results of the numerical calculations in two dimensions were scaled by a single factor. This factor was chosen such that overall the numerical results fit well with the analytical results. The above calculations were done with the same parameters as Fig. 1.

It is important to note that the expression for the differential cross section by Brown and Kibble was derived in three dimensions, but our calculations are for the differential cross length in two dimensions. Upon comparison, we find that that our results are in good agreement with the Brown and Kibble's results up to a constant factor. There is also no significant change (see Fig. 3) in the agreement with Brown and Kibble's result because of the relativistic correction discussed in Sec. II B. Brown and Kibble had arrived at their results by solving the Dirac equation but our agreement with their results justifies the approximation with the TDSE.

It was found that the scattering probability for nonlinear Compton exhibits a second-order dependence on the intensity of the incoming EM field as expected and the scattering probability for Compton scattering exhibits a first-order dependence on the intensity of the incoming EM field. This behavior was observed over at least three orders of magnitude (up to 1000 a.u.) in the electric field.

B. Bound-electron case

Here we consider the case of bound electrons because of its relevance to Fuchs *et al.* [13]. Unlike the calculations for a free electron, here we adopt a 3D approach for the most part. It is to be noted that a 3D calculation can be done with relative ease for the case of a bound electron, as the grid needed for convergent solutions is smaller. Hence, it involves less memory and time computationally when compared to the case of a free electron.

While the method developed in Sec. II allows for flexibility with respect to the choice of potential, to keep things simple a softcore Coulombic potential of the following form is chosen:

$$V(\boldsymbol{r}) = \frac{-Z}{\sqrt{x^2 + y^2 + z^2 + a}}. \tag{23}$$

Here, Z is equal to the effective nuclear charge seen by the electron in atomic units. By varying this, we can model the scattering from bound electrons of different BE. The parameter a is included to avoid the singularity [27–30] at the origin. While it is preferable to minimize the value of this parameter, there are constraints that arise from the grid spacing.

With this potential, we proceed as per Sec. II and obtain the scattering probability, $P_{k,\epsilon}$ (see Fig. 4–7). From the scattering probability calculations for nonlinear Compton scattering for different bound-state parameters, two things should be noted. First, there *is* a momentum shift, albeit an insignificant one when compared to the shift measured by Fuchs *et al.* [13]. Second, Ref. [13] measured a redshift while the simulations show a blueshift. While the additional shift in Compton wavelength has been well documented and studied [31,32], interestingly we find that a similar shift occurs in nonlinear Compton as well.

We calculate the differential cross section for Compton and nonlinear Compton as a function of angle for a bound electron. When we compare the calculated linear Compton differential cross section with the Klein-Nishina formula [17], we find excellent agreement (see Fig. 8) despite it being a bound electron. Upon comparing the nonlinear Compton differential cross section with Brown and Kibble's result [7], we find
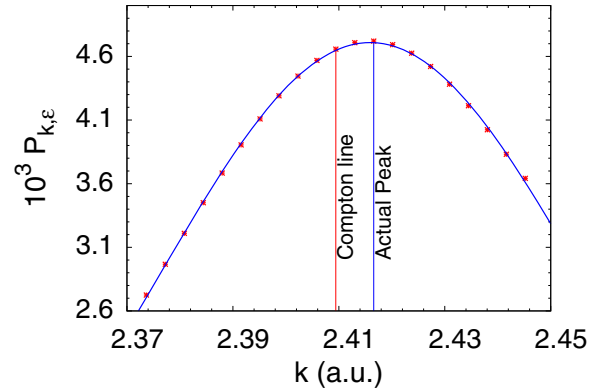

FIG. 4. The above plot was computed by solving the problem in two dimensions for $Z = 4$, $a = 0.1$ a.u., with a BE of 5.9593 a.u. at an angle of 130° and $t_{\mathrm{wid}} = 1$. It reveals the Compton defect in linear Compton scattering. The red vertical line and the blue vertical line indicate the expected peak (nonrelativistic) and the actual peak, respectively, in the scattered photon momentum k. The red points indicate the results of the numerical calculation and the blue curve indicates a Gaussian fit.

a general agreement (see Fig. 9). However, the calculated differential cross section for angles between 120° and 150° exhibits about 10% discrepancy. A part of this discrepancy arises from the fact that the Brown and Kibble formula used was nonrelativistic and therefore is missing factors of $\left(\frac{\omega_k}{\omega_{\mathrm{in}}}\right)$. The differential cross section for Compton scattering from Kibble and Brown is also missing these factors which were included in the Klein-Nishina formula. Therefore, it is difficult to determine the amount of error that originates from the numerical calculation and the amount that originates from the electrons being bound. These calculations were done for a range of values for Z and a and the results were found to be approximately the same.
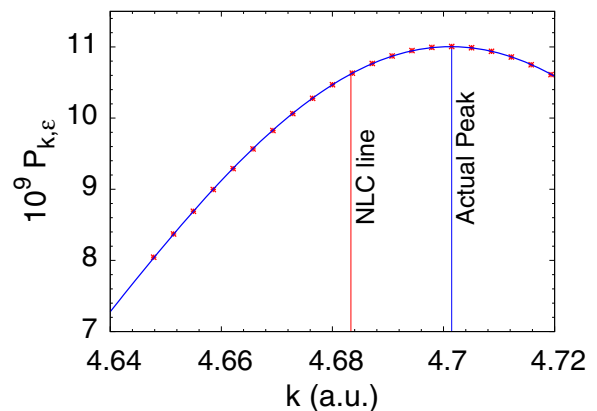

FIG. 5. The above plot was computed by solving the problem in two dimensions at an angle of 130° for $Z = 4$, $a = 0.1$ a.u. leading to a binding energy of 5.9593 a.u. The red points indicate the results of the numerical calculation and the blue curve indicates a Gaussian fit. It reveals an analog of the Compton defect in nonlinear Compton scattering. The red vertical line and the blue vertical line indicate the expected peak (nonrelativistic) and the actual peak, respectively, in the scattered photon momentum k. Here, $t_{\mathrm{wid}} = 1$.
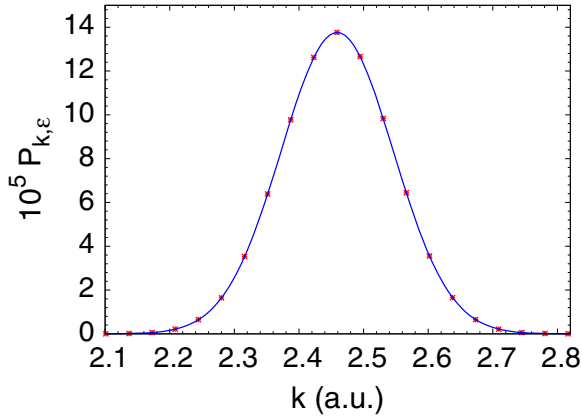
FIG. 6. Scattering profile for Compton scattering for a bound electron in three dimensions at an angle of $60°$ with $t_{\text{wid}} = 0.1$. The bound state of the electron is characterized by parameters $Z = 4$, $a = 0.1$ a.u. leading to a BE of 3.9496 a.u. The red points indicate the results of the numerical calculation and the blue line indicates a Gaussian fit.

It is to be noted that the results of Krebs *et al.* [15] are in terms of the double differential cross section and their double differential cross section has an extra frequency factor. Upon finding the area under their curve for double differential cross section by approximating it as a Gaussian and after accounting for differences in frequency, we find that our results are of the same order as theirs and agree to within a factor of ≈ 2. This comparison is approximate because the estimate for the area is crude due to the limited number of data points in the results of Ref. [15].

For all the calculations, the polarization of the scattered photon was in the same plane as that of the plane of polarization of the incoming photons. When the polarization of the
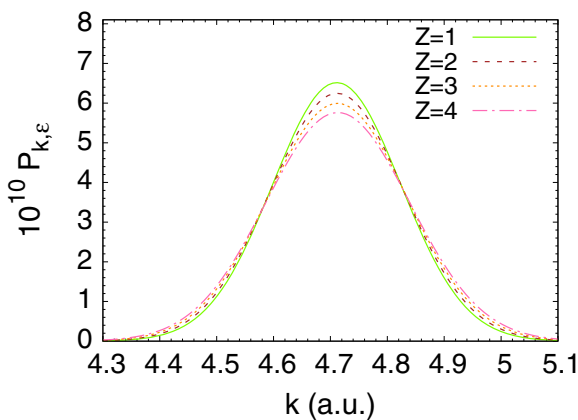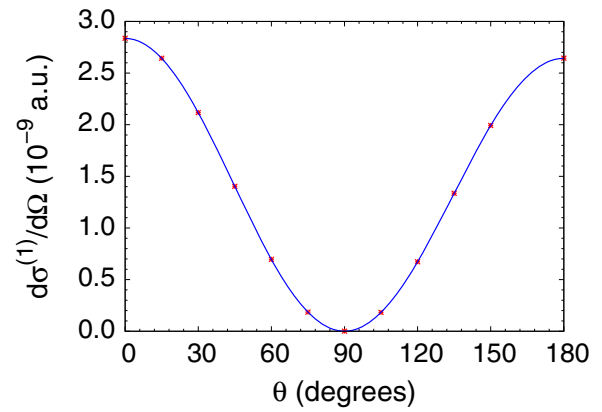

FIG. 8. Comparison of the differential cross section for Compton scattering from a bound electron as a function of scattering angle with the results of the Klein-Nishina formula. The red points indicate the results of the numerical calculation and the blue line indicates the results of the Klein-Nishina formula. The above calculations were done with the same parameters as in Fig. 6. All numerical calculations in three dimensions were done with no adjustable parameters.

scattered photon was chosen to be perpendicular to the plane of polarization of the incoming photons, the scattering probabilities were found to be more than six orders of magnitude smaller, for the case of nonlinear Compton scattering.

For calculating the additional shifts (defect) in k, we first numerically calculate the average k instead of obtaining the peak momentum from the Gaussian fit. When the polarization of the scattered photon is in the plane of polarization of the incoming photons,

$$k_{\text{avg}} = \frac{\sum_k k P_k}{\sum_k P_k}. \tag{24}$$

FIG. 7. Scattering profile for nonlinear Compton scattering for a bound electron in three dimensions at an angle of $120°$ with $t_{\text{wid}} = 0.1$. The figure contains the Gaussian fits from bound states characterized by $Z = 1, 2, 3,$ and 4 with binding energies (a.u.) 0.4037, 1.322, 2.5345, and 3.9449, respectively. Here $a = 0.1$, $E_C = 107$ a.u., $\omega_{\text{in}} = 340$ a.u. In the experiment in Ref. [13], the peak was observed at a k value of ≈ 4.5 a.u., but from the calculations the bound nature of the electron does not appear to have altered the peak scattered momentum from the free-electron value.
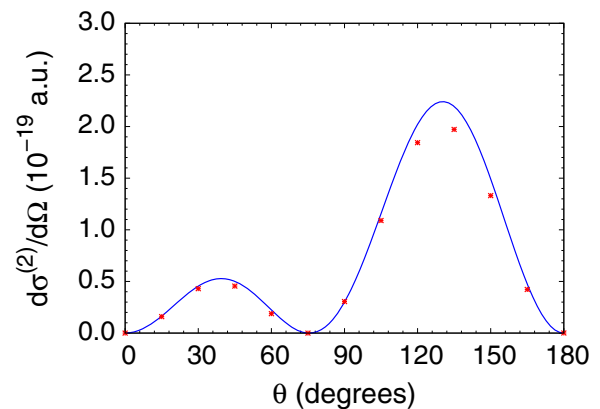

FIG. 9. Comparison of the differential cross section as a function of scattering angle for nonlinear Compton scattering from bound electrons with Brown and Kibble's free-electron result. The bound electron is characterized by parameters $Z = 4$ and $a = 0.1$ a.u. with a BE of 3.9496. The red points are a result of the numerical calculations in three dimensions while the blue line indicates the results of Brown and Kibble. The above calculations were done with the same parameters as Fig. 7. All numerical calculations in three dimensions were done with no adjustable parameters.

Here k_{avg} is the estimate for the scattered photon momentum that we use to calculate the defect, with respect to the theoretical nonrelativistic free-electron prediction for both linear and nonlinear Compton scattering. Because the x rays in the calculation have a Gaussian time dependence, the final momentum distribution is the convolution of the infinite resolution distribution with a Gaussian. The average of the final k is unchanged by the convolution because the Gaussian is a symmetric function while the peak value does slightly shift with the t_{wid}. In the calculations here, the scattering probability falls off slower than a Gaussian distribution for k values far from that for free-electron linear and nonlinear Compton scattering, which leads to small shifts. The underlying cause for this lies in the nature of the Compton profile of the bound electron. Following this, Richardson's extrapolation method [26] is used to obtain an estimate for the defect in scattered photon momentum after accounting for the numerical error from the grid spacing to the leading order. For the cases of $Z = 1, 2, 3,$ and 4 with $a = 0.1$, the defects were found to be of the size of $\approx 10^{-3}$ a.u. in k, which corresponds to an energy of about a few eV. It was found that the size of the defect increases with the binding energy of the electron. The defect was also found to be independent of the incident field over the range 1–110 a.u. of electric-field amplitude.

Let k_{final} and k_{initial} be the peak scattered momentum of the outgoing x-ray photon and the peak momentum of the incoming x-ray photons, respectively. For the case of nonlinear Compton scattering from a free electron at an angle of $120°$, $k_{\text{final}} - k_{\text{initial}} \sim -0.25$ a.u. From the experiment [13], $k_{\text{final}} - k_{\text{initial}} \sim -0.5$ a.u. From our bound-electron calculations, we find that $k_{\text{final}} - k_{\text{initial}} \sim -0.25$ a.u. but there is a small blueshift correction to this which is of the size $\approx +10^{-3}$ a.u. From these results, it is evident that the bound nature of the electron cannot explain the anomalous shift observed in Ref. [13].

C. Electron-electron correlation effects

We examine if electron-electron interaction effects could contribute to the redshift in the nonlinear Compton scattering. This can be done by a simple extension of the procedure developed in Sec. II. The Hamiltonian is modified to include the mechanical momentum from each electron and an interaction potential is introduced.

The modified Hamiltonian is given by

$$\hat{H} = \frac{[\hat{\boldsymbol{P}}_1 + \hat{\boldsymbol{A}}(\boldsymbol{r}_1)]^2}{2} + \frac{[\hat{\boldsymbol{P}}_2 + \hat{\boldsymbol{A}}(\boldsymbol{r}_2)]^2}{2} + V(\boldsymbol{r}_1) + V(\boldsymbol{r}_2)$$
$$+ \frac{1}{\sqrt{(x_1 - x_2)^2 + (y_1 - y_2)^2 + a}}$$
$$+ \sum_{\boldsymbol{k},\boldsymbol{\epsilon}} \omega_k \hat{a}_{\boldsymbol{k},\boldsymbol{\epsilon}}^\dagger \hat{a}_{\boldsymbol{k},\boldsymbol{\epsilon}}. \tag{25}$$

Here $\boldsymbol{r}_1$ and $\boldsymbol{r}_2$ refer to the position vectors of the electrons and $V(\boldsymbol{r}_1)$ and $V(\boldsymbol{r}_2)$ are the 2D equivalents of the expression in Eq. (23). The wave-function ansatz remains the same except that the quantities $\psi^{(0)}$ and $\psi_{\boldsymbol{k},\boldsymbol{\epsilon}}^{(1)}$ are now functions of both $\boldsymbol{r}_1$ and $\boldsymbol{r}_2$ along with time t.

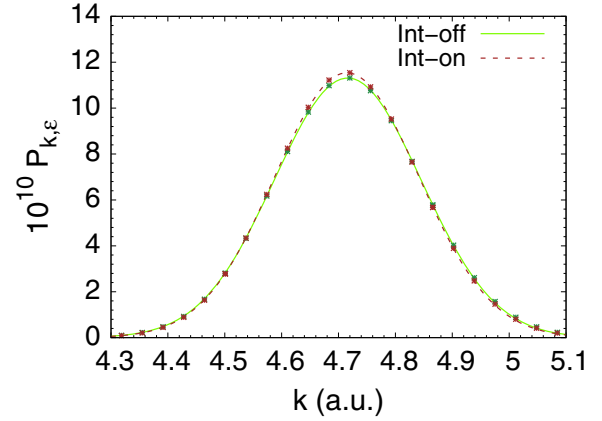With this approach, the calculations have to be restricted to two dimensions because of the time and space required

FIG. 10. Scattering profile for nonlinear Compton scattering for an angle of $130°$. The curves represent Gaussian fits while the points are the result of the numerical calculation. The dark green points and the green curve represent the case with the electron-electron interaction turned off and the brown points and the brown dotted line indicate the case with the interaction turned on. Here $Z = 4$, $a = 0.1$, $E_C = 107$ a.u., $\omega_{\text{in}} = 340$ a.u., $t_{\text{wid}} = 0.1$ a.u.

to handle the problem computationally. Restricting the calculation to two dimensions is reasonable given that there was not any significant difference in the 2D and 3D results from Secs. III A and III B, respectively.

The same numerical procedure discussed in Sec. II D is used to obtain the scattering probability $P_{\boldsymbol{k},\boldsymbol{\epsilon}}$ as a function of scattered photon momentum k. A comparison of the calculation with and without the electron-electron interaction does not indicate any significant change (Fig. 10).

This calculation is performed with a grid spacing of 0.14 a.u. and therefore it is not converged to the same extent as the previous calculations. In single bound-electron calculations in two and three dimensions, there is no substantial change in the nature of our results as the grid spacing is decreased from 0.2 to 0.07 a.u. We extrapolate from this trend and argue that the electron-electron correlation effects are unlikely to be the cause of the redshift observed in the experiment by Fuchs *et al.* [13].

D. Semi-Compton process

We consider a process where a bound electron absorbs an incoming photon and the now-ionized electron scatters another incoming photon inelastically to give rise to a photon of frequency $\approx 2\omega_{\text{in}}$. The electron ends up being recaptured by the atom during the process. This process should manifest itself in the calculations if the grid spacing was decreased enough to access the energy range in the continuum of the ionized electron. When the bound electron absorbs a photon, it gains a momentum of ≈ 26 a.u. This would not be represented in a grid with a spacing of 0.1 a.u., hence we consider a grid spacing of 0.02 a.u.

We resort to a 2D calculation to probe such a fine grid. The calculations do not reveal any significant difference in the scattering profile. We also consider the effect of binding energy on this scattering profile by decreasing the parameter a in the potential. We do not find any significant effect beyond

the Compton defect discussed in Sec. III B which is at least two orders of magnitude smaller than the shift observed by Fuchs *et al.* [13].

IV. CONCLUSION AND SUMMARY

We described a method to numerically calculate the linear and nonlinear Compton effect for free or bound electrons. The results from the calculation can be used to determine whether the bound nature of the electrons is caused the anomalous frequency shift observed in the experiment by Fuchs *et al.* [13]. To justify the approximations we compared our free-electron results with the analytical expressions available for differential cross sections of Compton [16,17] and nonlinear Compton scattering [7]. We found excellent agreement in those cases.

We employed a Coulombic interaction potential to model bound electrons and obtained their differential cross sections for Compton and nonlinear Compton scattering. Despite the electrons being bound, the calculations for the differential cross section agreed with the Brown and Kibble results. The calculations did not exhibit a redshift in the wavelength of the scattered photon, in disagreement with the experiment [13] but in agreement with the calculations of Krebs *et al.* [15]. For bound electrons, we also found the small expected blueshift in the case of Compton scattering and interestingly a

blueshift in the case of nonlinear Compton scattering as well. Our calculations support the conclusion in Ref. [15] that it is not the bound character of the electron that is causing the anomalous frequency shift seen in Fuchs *et al.* [13].

The role of electron-electron correlation effects on the redshift was explored by doing a two-electron calculation in two dimensions. The results of the calculation did not indicate the presence of the redshift in Ref. [13]. Following this, we considered the case of a semi-Compton process where linear Compton scattering occurs off of an ionized electron with the electron getting recaptured. This could give rise to a photon of frequency of $\approx 2\omega_{in}$. A calculation accounting for this process did not exhibit a redshift similar to the one observed in the experiment by Fuchs *et al.* [13]. No calculations have yet been able to reproduce the shift observed in Ref. [13].

[1] W. G. Cross and N. F. Ramsey, The conservation of energy and momentum in Compton scattering, Phys. Rev. **80**, 929 (1950).

[2] Z. Bay, V. P. Henri, and F. McLernon, Simultaneity in the Compton effect, Phys. Rev. **97**, 1710 (1955).

[3] B. I. Lundqvist and C. Lydén, Calculated momentum distributions and Compton profiles of interacting conduction electrons in lithium and sodium, Phys. Rev. B **4**, 3360 (1971).

[4] P. Eisenberger and P. M. Platzman, Compton scattering of X rays from bound electrons, Phys. Rev. A **2**, 415 (1970).

[5] M. J. Cooper, M. Cooper, P. E. Mijnarends, P. Mijnarends, N. Shiotani, N. Sakai, and A. Bansil, *X-Ray Compton Scattering* (Oxford University, New York, 2004), Vol. 5.

[6] L. Ball and J. G. Kirk, Probing pulsar winds using inverse Compton scattering, Astropart. Phys. **12**, 335 (2000).

[7] L. S. Brown and T. W. B. Kibble, Interaction of intense laser beams with electrons, Phys. Rev. **133**, A705 (1964).

[8] Vachaspati, Harmonics in the scattering of light by free electrons, Phys. Rev. **128**, 664 (1962).

[9] P. Emma, R. Akre, J. Arthur, R. Bionta, C. Bostedt, J. Bozek, A. Brachmann, P. Bucksbaum, R. Coffee, F.-J. Decker *et al.*, First lasing and operation of an ångstrom-wavelength free-electron laser, Nat. Photon. **4**, 641 (2010).

[10] T. Ishikawa, H. Aoyagi, T. Asaka, Y. Asano, N. Azumi, T. Bizen, H. Ego, K. Fukami, T. Fukui, Y. Furukawa *et al.*, A compact X-ray free-electron laser emitting in the sub-ångström region, Nat. Photon. **6**, 540 (2012).

[11] K. Tamasaku, E. Shigemasa, Y. Inubushi, T. Katayama, K. Sawada, H. Yumoto, H. Ohashi, H. Mimura, M. Yabashi,

K. Yamauchi *et al.*, X-ray two-photon absorption competing against single and sequential multiphoton processes, Nat. Photon. **8**, 313 (2014).

[12] G. Doumy, C. Roedig, S.-K. Son, C. I. Blaga, A. D. DiChiara, R. Santra, N. Berrah, C. Bostedt, J. D. Bozek, P. H. Bucksbaum *et al.*, Nonlinear Atomic Response to Intense Ultrashort x Rays, Phys. Rev. Lett. **106**, 083002 (2011).

[13] M. Fuchs, M. Trigo, J. Chen, S. Ghimire, S. Shwartz, M. Kozina, M. Jiang, T. Henighan, C. Bray, G. Ndabashimiye *et al.*, Anomalous nonlinear X-ray Compton scattering, Nat. Phys. **11**, 964 (2015).

[14] C. Bula, K. T. McDonald, E. J. Prebys, C. Bamber, S. Boege, T. Kotseroglou, A. C. Melissinos, D. D. Meyerhofer, W. Ragg, D. L. Burke *et al.*, Observation of Nonlinear Effects in Compton Scattering, Phys. Rev. Lett. **76**, 3116 (1996).

[15] D. Krebs, D. A. Reis, and R. Santra, Time-dependent QED approach to x-ray nonlinear Compton scattering, Phys. Rev. A **99**, 022120 (2019).

[16] J. M. Guilarte and M. Mayado, QED_2+ 1: The Compton effect, arXiv:hep-th/0009003 (2000).

[17] O. Klein and Y. Nishina, The scattering of light by free electrons according to Dirac's new relativistic dynamics, Nature (London) **122**, 398 (1928).

[18] Y. Pan and A. Gover, Spontaneous and stimulated emissions of a preformed quantum free-electron wave function, Phys. Rev. A **99**, 052107 (2019).

[19] Rodney Loudon, *The Quantum Theory of Light* (Oxford University, New York, 1983).

[20] C. Cohen-Tannoudji, B. Diu, and L. Franck, *Quantum Mechanics (Mecanique Quantique)*, Revised English ed. (Hermann, Paris, 1978), Vol. 2.

[21] J. W. Gibbs, Fourier's series, Nature (London) **59**, 200 (1898).

[22] T. K. Lindblom, M. Førre, E. Lindroth, and S. Selstø, Semirelativistic Schrödinger Equation for Relativistic Laser-Matter Interactions, Phys. Rev. Lett. **121**, 253202 (2018).

[23] M. Førre, Breakdown of the nonrelativistic approximation in superintense laser-matter interactions, Phys. Rev. A **99**, 053410 (2019).

[24] D. J. Bamford, L. E. Jusinski, and W. K. Bischel, Absolute two-photon absorption and three-photon ionization cross sections for atomic oxygen, Phys. Rev. A **34**, 185 (1986).

[25] Farhad HM Faisal, *Theory of Multiphoton Processes* (Springer, New York, 2013).

[26] W. H. Press, S. A. Teukolsky, and W. T. Vetterling, *Numerical Recipes in C: The Art of Scientific Computing*, 2nd ed. (Cambridge University, Cambridge, England, 1992).

[27] K. J. LaGattuta, Laser effects in photoionization: Numerical solution of coupled equations for a three-dimensional Coulomb potential, JOSA B **7**, 639 (1990).

[28] S. X. Hu and L. A. Collins, Intense laser-induced recombination: The inverse above-threshold ionization process, Phys. Rev. A **70**, 013407 (2004).

[29] A. Kołakowska, M. S. Pindzola, F. Robicheaux, D. R. Schultz, and J. C. Wells, Excitation and charge transfer in proton-hydrogen collisions, Phys. Rev. A **58**, 2872 (1998).

[30] A. Gordon, C. Jirauschek, and F. X. Kärtner, Numerical solver of the time-dependent Schrödinger equation with Coulomb singularities, Phys. Rev. A **73**, 042505 (2006).

[31] P. M. Bergstrom, Jr., Compton scattering of photons from electrons bound in light elements, Report No. ANL/PHY–94/1, Argonne National Laboratory, 1994.

[32] F. Bloch, Contribution to the theory of the Compton-line, Phys. Rev. **46**, 674 (1934).